EAI Endorsed Transactions
on Energy Web
Research Article EAI.EU

Image Recognition of Photovoltaic Cell Occlusion Based on Subpixel Matching

Yuexin Jin[1,a], Jinchi Yu[1,b], Xiaoju Yin[1,c*], Yuxin Wang[2,d*]

[1]Department of Renewable Energy, Shenyang Institute of Engineering, Shenyang, 110136, China
[2]Collage of Computer and Information Engineering, Tianjin Agricultural University, Tianjin, 300387, China

Abstract

INTRODUCTION: During the operation of large photovoltaic power stations, they are often shielded by dust and bird droppings, which greatly reduce the power generation and even cause fires. Analysis of PV cell occlusion image recognition accuracy based on sub-pixel matching.
OBJECTIVES: In order to find the location of the pv cells, we use the method of subpixel image matching. Improve recognition accuracy.
METHODS: When the power plant is running normally, taken the original image for photovoltaic power station as the original sample, and then using the subpixel gradient matching algorithm, to match the original image and find out that the minimum matching values.
RESULTS: If the calculation results is greater than a specified threshold, When the calculated result is greater than the specified threshold, the power station is considered abnormal.
CONCLUSION: The experimental process shows that this method can better judge the operating status of photovoltaic power station, and can find out the location of mismatched photovoltaic cells more accurately, and the calculation accuracy reaches sub-pixel level.

Keywords: subpixel; Photovoltaic cells; Shelter; Gradient matching algorithm; image recognition

Received on 18 November 2023, accepted on 5 April 2024, published on 12 April 2024

doi: 10.4108/ew.5751

1. Introduction

Photovoltaic plants need to operate for 25 years, during the operation, pv modules are often covered by bird droppings, dust, shadow, fallen leaves, snow. Due to the existence of local shielding, the current and voltage of some batteries change, then causing local temperature rise on these battery components, that is, the hot spot effect, cause the power generation greatly reduced, and even fire[1-2]. Local shielding and hot spot effecting can be detected by two methods: 1) The first method monitors mainly electrical components in photovoltaic cells and solar panel arrays. It is based on the principle of electrical characteristics in photovoltaic systems: when hot spots occur or solar cells are damaged, the electrical behavior of the cells in the photovoltaic system will change, thus affecting the current. and voltage changes. This method has high sensitivity and can detect minor faults to facilitate early discovery and maintenance; it does not require physical interference and does not damage the photovoltaic system. However, this method is costly and cannot provide comprehensive detection of reverser or connecting line problems;2) The second type focuses on partially occluded images. Based on image analysis and computer vision technology, it analyzes image color, shape, texture and other features. This method has a wide range of applications and has the advantages of image visualization for easy observation. However, it is affected by external conditions such as light, noise, etc., and it cannot detect solar cell performance and faults[3-6].

As there are many positions that are not easy to be found by naked eyes in large-area photovoltaic grid-connected power stations, so, at present, high-definition cameras and thermal imagers are used to acquire photovoltaic cell images and temperature values by unmanned aerial vehicles (UAVs), which can judge whether photovoltaic power stations generate electricity normally. In order to realize intelligent identification, many research methods have been proposed.

[a]474138758@qq.com, [b]1162675142@qq.com, [c*]Corresponding authors: Lnsolyxj@163.com, [d*]261235654@qq.com

Reference proposes an algorithm for hot spot identification using Gaussian filter and Laplacian operator, which can effectively identify the hot zone in solar panels[7-9]. Reference proposed a photovoltaic hot spot recognition algorithm combining threshold method and edge detection, which achieved good segmentation results[10]. Based on infrared technology, literature realized automatic recognition of hot spots by using the method of information fusion and fuzzy reasoning[11]. Reference reports that using prior knowledge to segment the panel area of photovoltaic hot spot image, can effectively avoid interference caused by background information on hot spot recognition and improve the subsequent recognition accuracy[12].

However, local occlusion such as dust and bird droppings will not cause temperature rise and hot spot effect in a short period of time, so it cannot be detected by temperature. Therefore, it is necessary to analyze and process photovoltaic cell images by high definition camera at the same time. In this paper, the sub-pixel matching method of images is adopted. First, the original image samples are taken in advance when the power station is running normally, and then the images to be detected and the original images are converted into grayscale images. Finally, the sub-pixel image matching is carried out to find the location of abnormal power generation.During the experiment, he normal photovoltaic cells, simulated photovoltaic cells blocked by bird droppings, and photovoltaic cells blocked by shadows were selected, the latter two images were matched with the first image, and the better calculation results were obtained, which can also be applied to the image processing of photovoltaic thermal imaging. This method is also suitable for hot spot recognition in infrared image.

2. Whole-pixel point image matching

Finding the best matching block for each part Gi in the original graph. Assuming that $i = 1,2,3,4$, the pixel value of each pixel point of the graph Gi to be detected is $g_i(x, y)$, the mean value with the line, and the center point is $P_i(X_i, Y_i)$; The pixel value of each pixel point in the original figure is $g_i(x, y)$, the mean value with the line, the center point is $P_1(X_1, Y_1)$, and the number of rows and columns in the pixel point matrix of the matching figure is M and N, then it can be concluded[9]:

$$C(p_i) = \frac{1}{M \times N} \sum_{j=1}^{N} \sum_{i=1}^{M} \sqrt{\left[\left| g(x,y) - \overline{g(x,y)} \right| - \left| f(x_1,y_1) - \overline{f(x_1,y_1)} \right|^2 \right]} \quad (1)$$

When the obtained value is the smallest $C(p_i)$, the similarity of the sub-region on the matched result graph is the highest, then obtained matching region of the whole pixel, and the displacement of the center point is:

$$(u_i, v_i) = (X_i - X_1, Y_i - Y_1) \quad (2)$$

3. Sub-pixel point image matching

(i) Calculation of sub-pixel point values

First, calculating the values of the sub-pixel points, and setting the values of the four whole pixel points surrounding the sub-pixel points: the original figure is f_1, f_2, f_3, f_4, and the matching diagram g_1, g_2, g_3, g_4,the values of the sub-pixel points: the original figure is f_i,the matching diagram is g_i, the interval distance between the pixels is R, the distance between the sub-pixel and the boundary is h_1 and h_2, as shown in Figure 1. the value of the sub-pixel points f_i can be obtained as follows[12]:

$$A = \frac{R - h_1}{R} f_1 + \frac{h_1}{R} f_3 \quad (3)$$

$$B = \frac{R - h_1}{R} f_2 + \frac{h_1}{R} f_4 \quad (4)$$

$$f_i = \frac{R - h_2}{R} A + \frac{h_2}{R} B \quad (5)$$

Similarly, the value of sub-pixel points can be obtained as:

$$C = \frac{R - h_1}{R} g_1 + \frac{h_1}{R} g_3 \quad (6)$$

$$D = \frac{R - h_1}{R} g_2 + \frac{h_1}{R} g_4 \quad (7)$$

$$g_i = \frac{R - h_2}{R} C + \frac{h_2}{R} D \quad (8)$$

In Figure 1, Figure 1 (a) expresses the relationship between sub-pixel points and whole pixel points intuitively with the formula, while Figure 1 (b) expresses the relationship between sub-pixel points and whole pixel points with the simulation image. The two adjacent pixels are represented by a blue square in Figure 1 (b), and what is invisible to the naked eye between these two pixels is the sub-pixel point, which is represented by a red dot in the image, and each pixel is regarded as four pixel points from the horizontal and vertical aspects. The accuracy of the sub-pixel points in this figure is set to one quarter in order to improve the resolution.

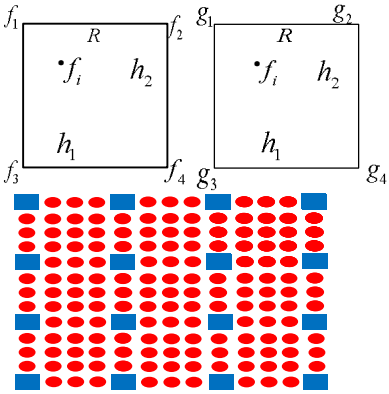

(a) The relationship between the two formulas (b) The relationship between the two pixels

Figure 1. Relationship between sub-pixel points and whole pixel points

(ii) Sub-pixel point matching $X_1 = X + u + dx$ and $Y_1 = Y + v + dy$, plug them into formula (1), take partial derivatives of dx and dy respectively, and set the derivatives to zero, it can be concluded that[13]:

$$\begin{pmatrix} d_x \\ d_y \end{pmatrix} = \begin{pmatrix} \sum\sum g_x * g_x & \sum\sum g_y * g_x \\ \sum\sum g_y * g_x & \sum\sum g_y * g_y \end{pmatrix}^{-1} * \begin{pmatrix} \sum\sum (f-g) * g_x \\ \sum\sum (f-g) * g_y \end{pmatrix} \quad (9)$$

Through cubic spline interpolation, it can be concluded that:

$$g_x = \frac{1}{12} * g(x-2,y) - \frac{8}{12} * g(x-1,y) + \frac{8}{12} * g(x+1,y) - \frac{1}{12} * g(x+2,y) \quad (10)$$

$$g_y = \frac{1}{12} * g(x,y-2) - \frac{8}{12} * g(x,y-1) + \frac{8}{12} * g(x,y+1) - \frac{1}{12} * g(x,y+1) \quad (11)$$

The values of dx and dy can thus be calculated, and the location of the subpixel matching point that minimizes the value can be determined[14-15]

4. Segmentation and matching method based on sub-pixel

In this paper, the segmentation matching algorithm is adopted to match the matching graph with the original graph. The specific process of the detection algorithm is as follows:
(i) The whole pixel is matched firstly to find the matching point of the whole pixel;

(ii) Calculating the mean value of each image pixel, setting the original image as X and match the graph Y_i, where $I = 1,2,3,4$. Normalize each image to eliminate the influence of different average pixel values again: Set the original value as Pi and the normalized value as Q_i, then:

$$Q_i = \frac{X}{Y_i} * P_i \quad (12)$$

(iii) Calculating the maximum value M and minimum value S of the obtained values of each image, and the mean difference:

$$JC = \frac{M - S}{S} \quad (13)$$

(iv) If the JC calculation result is greater than the pre-specified threshold, it is considered that the photovoltaic cell is abnormal and the detection of the cell is completed.

(v) When JC value is less than the pre-specified threshold value, namely, normal photovoltaic cells are detected, and the matching graph is divided into four equal parts, denoted as G_1, G_2, G_3, G_4 respectively. The original graph remains unchanged, as shown in Figure 2. Then, the best matching speed is founded in the original image for sub-pixel matching, so as to calculate the position of sub-pixel matching points[16].

(vi) JC value is also calculated. If JC value is less than the pre-specified threshold value, it is divided into four equal parts and the matching process is repeated. When the JC value of all four photovoltaic cells is greater than the pre-specified threshold or the segmented image is too small to be divided any more, the detection is considered to be completed. Finally, the position of the matched block that does not meet the accuracy is determined as the position of the abnormal photovoltaic cell[17-18], as shown in Figure 3.

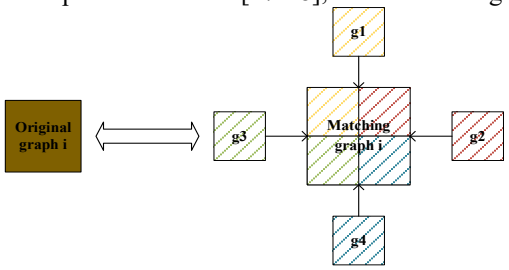

Figure 2. Segmentation matching process

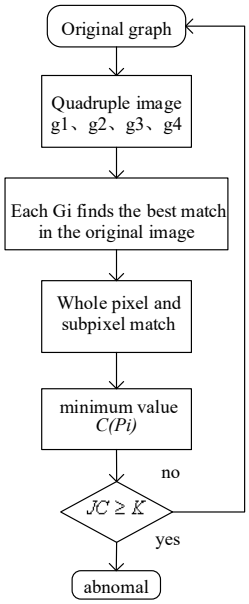

Figure 3. Process of segmentation matching algorithm

5. Application examples

The experimental process is as follows:

(i) Obtain detection images

The monitoring camera device is installed at fixed points. First, the original image is obtained. In the initial state or normal operation of the photovoltaic power station, the original sample image F is obtained with pixel value $f(x,Y)$; Then the detected image is obtained, and the detected image sample G with pixel valueb $g(x,Y)$ is periodically obtained to detect whether the photovoltaic cell is abnormal; As the location of photographing is the same, the serial number, size, number and sequence of images taken have been fixed, so images in the same location and serial number can be matched[19-20], as shown in Figure 4.

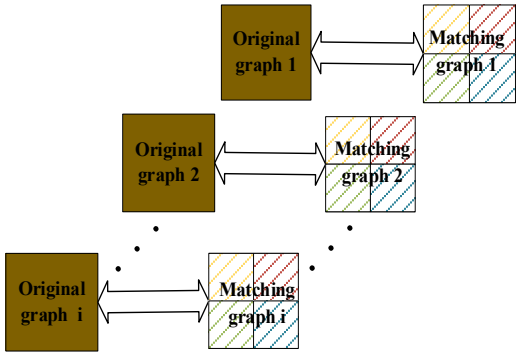

Figure 4. The original matches the detected image

In order to simplify the calculation we only selects the single panel for matching. Figure 5 (a) is the photovoltaic cell under normal conditions, namely the original image sample, and Figure 5 (b) (c)is the sample to be detected[21-22]. Figure 5 (c) is simulated samples covered by mud and bird droppings. The image is actually shot at the photovoltaic power station. The white light in the upper right corner is actually reflected light from the sun, and the black in the lower left corner of the image is shielding from the shooting Angle, which is not a failure of the panel, so it needs to be de-dryness processing.

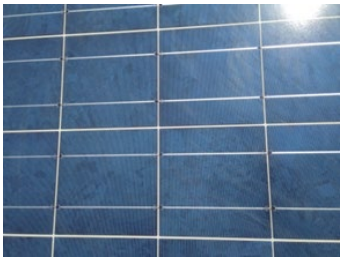

(a) Normal image

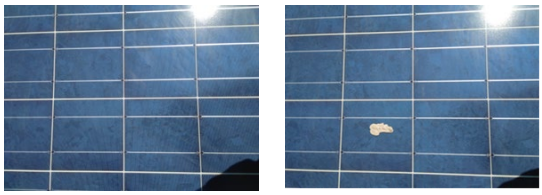

(b) Detection image

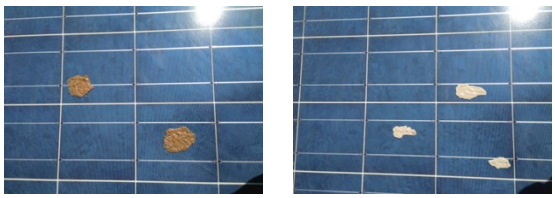

(c) Detection image (Bird droppings and dirt)

Figure 5. Original and detection image sample

(ii) Convert to grayscale image

The image is converted to grayscale image, and Figure 6(a) is normal grayscale image, Figure 6(b) is the gray scale to be detected, and Figure 6(c) is the gray level of soil and bird droppings shielding the solar panel.

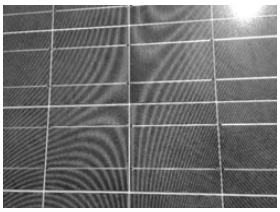

(a) Normal image gray scale

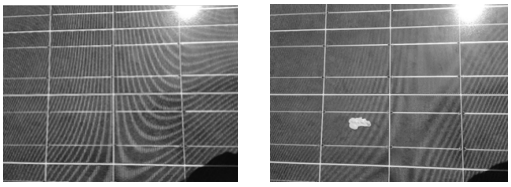

(b) Grayscale of the image to be detected

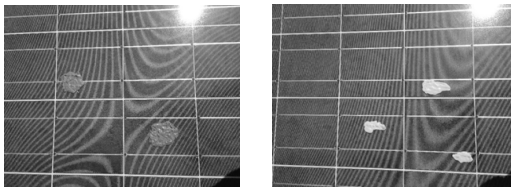

(c) Gray scale of soil and bird droppings occlusion

Figure 6. Original and detected gray image

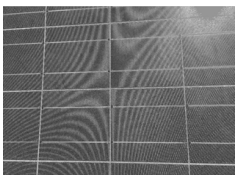

(a) Normal image denoising

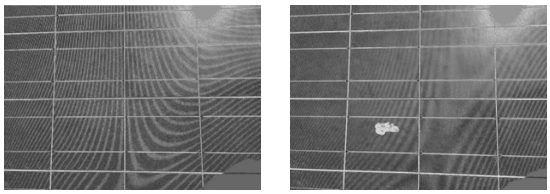

(b) Detection of image gray processing

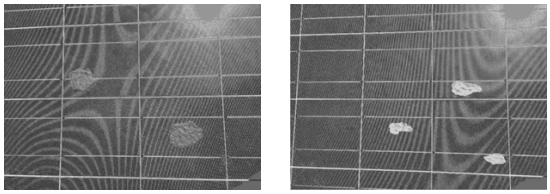

(c) Soil and bird droppings occlusion denoising processing gray scale

Figure 7. Original and detected image after denoising

(iii) Image denoising

Firstly, the image needs to be de-noised. The noise here is mainly white light caused by strong light radiation, and black part caused by occlusion. The figure after de-noising is shown in Figure 7.Remove the white strong light in the upper right corner ,When the pixel value is greater than or equal to 220, make the pixel value equal to 150, remove the black occlusion at the bottom right corner

The method is firstly to calculate the mean value of each pixel of grayscale image, and the calculation formula is as follows:

Where M and N are the number of rows and columns of the matrix, M=3456; N = 4608. When the pixel value is less than or equal to 50, make the pixel value equal to the pixel mean, namely:

$$f(i,j) = C(p), \text{if} f(i,j) \le 50 \quad (14)$$

The denoising pre-processing method is applied to the above images. Figure 7 (a) shows the denoising processed image of the normal image. Figure 7 (b) is the image after denoising of the image to be detected; Figure 7 (c) Denoising image of multiple soil and bird droppings occlusion

(iv) Segmentation and matching of whole pixel images[23-24]

Firstly, the mean value of each image pixel in Figure.7 was calculated as (1)X=105.5223;(2)Y_1=103.5130;(3) Y_2=108.2600;(4)Y_3=103.6789;(5)Y_4=107.5382.By using formula (1) to match whole pixels[25], the matching result image of the original image and matching image in Figure 8 can be obtained, as shown in. Figure 8 (a) shows the whole pixel matching diagram of the gray level image to be detected; Figure 8 (b) shows the full-pixel matching diagram of soil and bird droppings occlusion gray image.

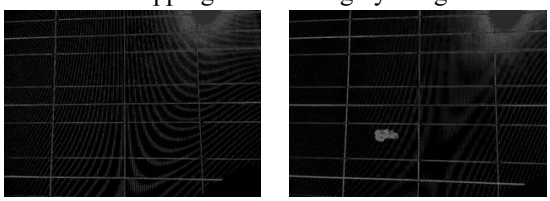

(a) Whole pixel matching result image

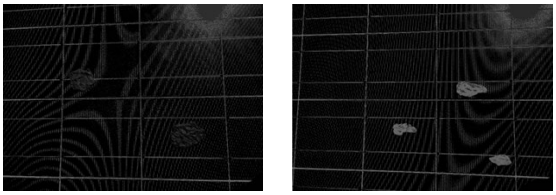

(b) Multi-occlusion full pixel matching results image

Figure 8. The results of pixel matching in normal image were compared

The matching values of the original graph and matched graph in Figure. 8 are shown in the first row of Table 1.Each image

is normalized to eliminate the influence of different average pixel values again: Let the original value be P_i and the normalized value be Q_i, then:

$$Q_i = \frac{X}{Y_i} * P_i \tag{15}$$

Where I =1, 2, 3, 4; See the first row in Table 2.

(v) Sub-pixel image segmentation and matching

As shown in Figure 9, divided the matching image into four equal partsthe coordinates of the upper left corner of the four parts divided are (1,1) (m,1) (1,n) (m,n). Again, through the subpixel matching formula(9), (10) and (11), In Figure 7(a), finding the best sub-pixel matching block for matching. Each sub-pixel matching value is given in Table 1 to Table 3.

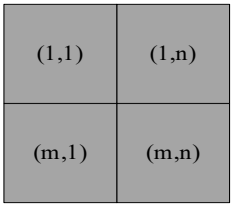

Figure 9. Split and Match Schematic

Table 1. Whole pixel matching and sub-pixel matching values of the first segmentation

	①~②	①~②	①~④	①~⑤
Total	10.2240	9.6466	10.4987	11.6307
First	11.1091	9.1904	10.7206	11.8639
Second	12.2451	11.9811	12.4744	14.1289
Third	7.9812	6.6308	8.0153	9.0177
Fourth	10.5084	11.3668	12.3224	13.157

Table 2. Normalized whole-pixel matching and sub-pixel matching values of the first segmentation

	①~②	①~②	①~④	①~⑤
Total	10.0293	9.8969	10.3153	11.8529
First	10.8976	9.4288	10.5333	12.0905
Second	12.2451	11.9811	12.4744	14.1289
Third	7.8292	6.8028	7.8753	9.1899

Calculating the mean value T, maximum value M, minimum value S, the difference between maximum and minimum value $M-S$, and the mean difference value $JC=(M-S)/S$ of all values in Table 2; When mean difference $JC \geq 1.2$, it indicates the panel is shielded. Due to the small difference between gray values of the third panel occlusion position and other positions, the occlusion phenomenon cannot be detected, further processing such as image sharpening or image enhancement is needed to correctly detect the fault.

Table 3. Calculated values

	First	Second	Third	Fourth
maximum	13.0336	12.7862	13.1458	16.0761
minimum	6.8103	6.4211	7.1291	5.6674
mean	10.3181	9.9774	10.6645	12.359
difference value	6.2233	6.3651	6.0166	10.4086
average difference	0.9138	0.9913	0.8439	1.8365

6. Conclusion

In this paper, the sub-pixel image matching method is adopted to study the image of the blocked photovoltaic cell. The experimental results show that:

(i) This method uses sub-pixel level calculation accuracy for image matching calculations, allowing more detailed interpolation between pixels to avoid discretization errors and obtain smooth recognition results.

(ii) This algorithm normalizes the solar panel image, which is used to eliminate the influence of different average pixel values, improve the quality of image recognition, and ensure that the image recognition is not affected by external lighting factors.

(iii) By comparing the relationship between the JC value and the threshold, the image will continue to be divided if it is not satisfied. The rigorous matching process ensures that no omissions will occur in the detected solar panel blocked image.

Acknowledgements.

China University Innovation Fund -- New Generation Information Technology Innovation Key Project, No. 2022IT017; Education Reform Project of China Institute of Labor Electronicsin 2022, No.CIEL2022060; Cooperative Education Program ofMinistry of Education, No.220900287260151, No.202102602013;Key Project of Graduate Education and Teaching Research andReform of Tianjin Agricultural University, No. 2021-YA-6; Talent Support Program of Tianjin Agricultural University, No. Y0400907; School-enterprise cooperation technology researchand development project (TNHXKJ2022074, TNHXKJ2023009); Tianjin Graduate Research Innovation Program, No.2022Skyz258, 2022SKYZ261

References

[1] Guoli L,Fang W,Fei F, et al. Hot Spot Detection of Photovoltaic Module Based on Distributed Fiber Bragg Grating Sensor[J]. Sensors,2022,22(13).

[2] Lakshmi S P,Sivagamasundari S,Sri M R. IoT based solar panel fault and maintenance detection using decision tree with light gradient boosting[J]. Measurement: Sensors,2023,27.

[3] Kumar B K,Kumar A P. Detection and Classification of Faults in Solar PV Array Using Thevenin Equivalent Resistance[J]. IEEE Journal of Photovoltaics,2020,10(2)

[4] Shiguang S, Xiongxiong G, Wei R, et al. Hydrothermal synthesis and photovoltaic performance of silicon-based ZnO nanorods array heterojunction solar cells [J]. Rare Metal Materials and Engineering,2022,51(06):1993-1998.

[5] Mingli Z,Ran P,Baosheng L, et al. The Influence of Cryogenic Treatment on the Microstructure and Mechanical Characteristics of Aluminum Silicon Carbide Matrix Composites[J]. Materials, 2023,16(1).

[6] Soulayman S,Hamoud M,Hababa M, et al.Feasibility of Solar Tracking System for PV Panel in Sunbelt Region[J].Journal of Modern Power Systems and Clean Energy,2021,9(02):395-403.

[7] Hui G,Shan H,Fei W, et al. A novel method for quantitative fault diagnosis of photovoltaic systems based on data-driven[J]. Electric Power Systems Research,2022,210.

[8] Yongjie L,Kun D,Jingwei Z, et al. Intelligent fault diagnosis of photovoltaic array based on variable predictive models and I–V curves[J]. Solar Energy,2022,237.

[9] Naveen Venkatesh S;Sugumaran V Machine vision based fault diagnosis of photovoltaic modules using lazy learning approach[J]. Measurement,2022,191.

[10] R. P S,Sheetal B,Bhimgonda R P, et al. Reliability and Criticality Analysis of a Large-Scale Solar Photovoltaic System Using Fault Tree Analysis Approach[J]. Sustainability,2023, 15(5).

[11] Xie X,Ge S,Xie M, et al. An improved industrial sub-pixel edge detection algorithm based on coarse and precise location[J]. Journal of Ambient Intelligence and Humanized Computing,2019,11(5).

[12] Zhiguo D,Xiaobo W,Zhipeng M. Research on 3D model reconstruction based on a sequence of cross-sectional images[J]. Machine Vision and Applications,2021,32(4).

[13] Rui W,Kaiming Y,Yu Z. A high-precision Mark positioning algorithm based on sub-pixel shape template matching in wafer bonding alignment[J]. Precision Engineering,2023,80.

[14] Cheng H,Wei J,Qian X, et al. Sub-pixel Edge Detection Algorithm Based On Canny-Zernike Moment Method[J]. Journal of Circuits, Systems and Computers,2020,29(15).

[15] Cheng Z,Shuwen X,Yi H, et al.Nonlinear Sampled-Data Systems with a Generalized Hold Polynomial-Function for Fast Sampling Rates[J].Journal of Systems Science & Complexity, 2019,32(06):1572-1596.

[16] Wang J,Chen J. Subpixel edge detection algorithm based on improved Gaussian fitting and Canny operator[J]. Academic Journal of Computing & Information Science,2022,5.0(7.0).

[17] Bian X,Qinghua Z,Vincent B. On Quadratic Interpolation of Image Cross-Correlation for Subpixel Motion Extraction †[J]. Sensors,2022,22(3).

[18] Yu H,Xugang L,Fan W, et al. Non-Measuring Camera Monitoring of Comprehensive Displacement of Simulated Slope Mass Based on Edge Extraction of Subpixel Ring Mark[J]. Applied Sciences,2022,12(8).

[19] Yu H,Xugang L,Fan W, et al. Non-Measuring Camera Monitoring of Comprehensive Displacement of Simulated Slope Mass Based on Edge Extraction of Subpixel Ring Mark[J]. Applied Sciences,2022,12(8).

[20] Wang P,Guo X,Sang Y, et al. Measurement of local and volumetric deformation in geotechnical triaxial testing using 3D-digital image correlation and a subpixel edge detection algorithm[J]. Acta Geotechnica,2020,15(10).

[21] Mo J,Yan H,Liu J. An adaptive sub-pixel edge detection method based on improved Zernike moment[J]. International Journal of Wireless and Mobile Computing,2022,22(2).

[22] Haoran X,Junze H,Junru Z, et al. Displacement Measurement of Shaking Table Experiments Based on Binocular Vision and Subpixel Optimization[J]. Journal of Physics: Conference Series, 2023, 2577(1).

[23] Miaomin W, Fuyou X ,Yan X, et al. A robust subpixel refinement technique using self-adaptive edge points matching for vision-based structural displacement measurement[J]. Computer-Aided Civil and Infrastructure Engineering,2022, 38(5).

[24] Mu K, Yuanbo L. B-ultrasound image amplification algorithm based on binary polynomial interpolation [J]. Journal of Ningxia University (Natural Science Edition),2021, 42(02):117-121+128.

[25] Yi D, Guirong W, Liang H. Based on the improved gradient method of digital image correlation with sub-pixel displacement algorithm [J]. Journal of modern electronic technology, 2022, (17) : 29-34.